COMMUNICATIONS IN SCIENCE AND TECHNOLOGY
Homepage: cst.kipmi.or.id

Conductivity and mechanical properties of PEO/PVA/UiO-66 composite polymers for the membrane of lithium-ion batteries

Aep Patah*, Achmad Rochliadi, Aditya Husein, Dadang Ramadhan

Research Division of Inorganic and Physical Chemistry, Institut Teknologi Bandung, Bandung 40132, Indonesia

Article history:
Received: 28 August 2024 / Received in revised form: 22 November 2024 / Accepted: 27 November 2024

Abstract

Lithium batteries play a vital role in energy storage across electronics, transportation, and industrial sectors. Despite their importance, lithium-ion battery separators, such as Celgard, still need significant improvements, particularly in ionic conductivity (σ). A promising approach to enhance both conductivity and mechanical properties in lithium-ion batteries is the combination of Metal-Organic Frameworks (MOFs) and polymers. In this study, UiO-66 MOFs were synthesized through the solvothermal method at a temperature of 120°C. These MOFs were composited with polyethylene oxide (PEO) and polyvinyl alcohol (PVA) polymer membranes through the solution casting method. The UiO-66 MOFs/PEO/PVA polymer composites were created by varying the content of UiO-66 from 2% to 8% (w/w), while maintaining a constant lithium hexafluorophosphate ($LiPF_6$) concentration of 9% (w/w). The characterization of these composites was performed with the aid of X-ray Diffraction (XRD) and Fourier-Transform Infrared (FTIR) spectroscopy. Furthermore, to evaluate the performance of the composite membranes, Electrochemical Impedance Spectroscopy (EIS) tests and tensile tests were conducted. The resulting membrane with 6% (w/w) UiO-66 MOFs demonstrated an ionic conductivity (σ) of 5.60×10^{-3} S cm^{-1} and a tensile strength of 32.5 MPa. With its high ionic conductivity, this PEO/PVA/UiO-66 composite membrane holds a significant promise to be used as a separator membrane in lithium-ion batteries.

Keywords: MOFs; membrane; separators; lithium-batteries

1. Introduction

The global demand for electricity is projected to grow by approximately 3.4% annually from 2024 to 2026 [1]. This increasing demand will be entirely met by low-emission electricity sources. As a consequence, energy storage technology is deemed crucial to ensure the continual adoption of eco-friendly energy solutions [2]. Of various energy storage technologies, lithium-ion batteries [3,4] are extensively utilized in view of their numerous advantages, including a long lifespan [5], rapid recharging efficiency [6], lightweight and compact design [7], and lower toxicity in comparison to other types of batteries [8].

A lithium-ion battery consists of a number of main components, i.e. electrodes, electrolyte, and separator [9]. Of these components, separator is undergoing intensive development [10,11], given its critical role in separating the positive and negative electrodes [12], facilitating lithium-ion diffusion [13], preventing chain reactions that might lead to explosions [14], and enhancing battery conductivity [4]. Celgard, a widely used commercial separator [15], is a polymer membrane made from polyethylene (PE) and polypropylene (PP) [16]. It offers excellent electrochemical stability and mechanical strength [17]; however, its limited ionic permeability [18] has sparked a search for alternative materials to replace Celgard in battery separators.

Polyethylene oxide (PEO) has been being in investigation as a potential material for lithium-ion battery separators for its excellent thermal stability and ionic interface stability [19, 20]. It has low ionic conductivity and insufficient mechanical properties, however [21]. As a solution, researchers are now developing PEO-based composite membranes by blending PEO with other polymers or materials for battery applications. Recent studies have reported the following conductivity values for PEO-based composite membranes: PEO/polyvinyl alcohol (PVA) at 10^{-3} S cm^{-1} [19], PEO/imidazolium-derived ionic liquid at 1.87×10^{-4} S cm^{-1} [20], T/PVDF/PEO at 2.46×10^{-9} S cm^{-1} [22], PEO/Li_6PS_5Cl at 1.03×10^{-3} S cm^{-1} [23], and PEO/LLZTO at 3.23×10^{-4} S cm^{-1} [24]. A previous research revealed that PEO-based composites showed a significant potential for use as battery membranes in consideration to their promising conductivity values. Notably, PEO/PVA composites exhibit a number of key characteristics for battery membranes, such as good mechanical strength [19,21], thermal stability (with a decomposition temperature of approximately 300°C) [25,26], favorable surface wettability [27,28], and moderate conductivity [19]. However, further enhancements are deemed necessary to achieve the ideal

* Corresponding author.
Email: aep@itb.ac.id
https://doi.org/10.21924/cst.9.2.2024.1515

properties for battery membranes. One promising strategy to improve the performance of PEO/PVA composites is to incorporate materials such as metal-organic frameworks (MOFs) [29,30,31].

Metal-organic frameworks (MOFs) are the hybrid materials characterized by their large pores and surface areas, which enable them to be valuable for any applications in catalysis [19], drug delivery [32], and lithium-ion battery separators [33]. In MOFs, organic ligands create porous structures that not only can enhance the transport of lithium ions but also improve ionic conductivity in batteries [34]. Additionally, these frameworks can increase the energy capacity of batteries by facilitating the storage of lithium ions [18].

Research has demonstrated that composites made from CuBDC MOFs, polyethylene oxide (PEO), and LiTFSI can significantly boost ionic conductivity from 10^{-6} S cm^{-1} to 10^{-3} S cm^{-1} [19]. MOFs, therefore, have a considerable potential to enhance both ionic conductivity and energy capacity in lithium-ion batteries. Of the various types of metal-organic frameworks (MOFs), UiO-66 has emerged as a promising candidate for use in battery composite membranes. This is attributed to its excellent thermal stability with a decomposition temperature of approximately 500°C [35,36] as well as its high porosity, which facilitates the charge transfer [37]. UiO-66 also exhibits good wettability that can enhance ion diffusion [38,39]. As a result, incorporating UiO-66 into a composite membrane can provide a distinctive and innovative approach to improve the conductivity of lithium battery membranes made from polyethylene oxide (PEO) and polyvinyl alcohol (PVA) composites. However, it is important to note that the addition of MOFs can often lead to a decrease in the mechanical properties of the membrane.

This research aims to synthesize composite polymer electrolyte (CPE) membranes for lithium-ion battery applications using UiO-66 metal-organic frameworks (MOFs) and PEO/PVA polymers to enhance ion conductivity while evaluating the optimal concentration of UiO-66 MOF for improved mechanical properties.

2. Materials and Methods

2.1. Synthesis of MOFs UiO-66

The synthesis of UiO-66 MOF was performed through the solvothermal method. It began by dissolving 2 mmol of H_2BDC (0.3344 g) in 20 mL of DMF, while 2 mmol of $ZrCl_4$ (0.5396 g) was dissolved in 10 mL of DMF. These two solutions were subsequently combined, and the entire reaction process was conducted in a nitrogen (N_2) atmosphere. The mixture was sonicated for 45 minutes and heated in an oven at 120°C for 24 hours. After this period, the mixture was washed three times with chloroform. The produced white solid was filtered and stored at room temperature. To activate the UiO-66 MOFs, a degassing process was carried out for 6 hours at 250°C.

2.2. Synthesis of UiO-66/PVA/PEO composite membrane

The synthesis of the composite electrolyte membrane was carried out via the casting method. Polyethylene oxide (PEO) and polyvinyl alcohol (PVA) were initially mixed in a 1:4 weight/weight ratio, specifically 0.15 g of PEO and 0.75 g of PVA, and dissolved separately in 10 mL of distilled water. The polymer solutions were then stirred for 6 hours and heated to 55°C for PEO and 70°C for PVA. Once the two polymer solutions were combined, lithium salt ($LiPF_6$) was added, making up 9% of the total polymer weight, along with varying amounts of UiO-66 metal-organic frameworks (MOFs). The UiO-66 MOFs were incorporated in different proportions: 0%, 2%, 4%, 6%, and 8% of the polymer weight. The produced mixture was then cast into Teflon molds to form the membrane.

2.3. Characterization of UiO-66/PVA/PEO composite membrane

The characterization of the MOFs was conducted by means of X-Ray Diffraction (XRD) analysis to investigate the structural properties of UiO-66 MOFs and the UiO-66/PEO/PVA composite membrane. This analysis was performed over a 2θ range of 5° to 50°. Additionally, Fourier-Transform Infrared (FTIR) spectroscopy measurements were carried out to identify the functional groups present in the UiO-66/PEO/PVA polymer composite membrane.

2.4. Conductivity test of UiO-66/PVA/PEO composite membrane

Conductivity can be assessed by measuring either resistance or impedance. Electrochemical Impedance Spectroscopy (EIS) is a highly effective method for measuring impedance. For this purpose, we then used the Gamry Reference 3000 Potentiostat/Galvanostat. The measurements were performed in Galvanostat mode with frequency parameters in the range of 1 MHz to 0.1 Hz and a current set at 0.5 mA. The EIS measurement was conducted on a membrane with the dimensions of 3 × 2 × 0.04 cm.

2.5. Mechanical test of UiO-66/PVA/PEO composite membrane

Tensile strength test was performed to evaluate the mechanical properties of the UiO-66/PEO/PVA polymer composite membrane. This test aimed to determine how the addition of UiO-66 determined the tensile strength of the composite membrane. For this evaluation, the UiO-66/PEO/PVA polymer composite membrane was tested using a TENSOLAB-5000 at room temperature. Here, the UiO-66/PEO/PVA polymer composite membrane was subjected to tensile testing using a TENSOLAB-5000 at room temperature conducted on a sample measuring 10 mm in length and 0.11 mm in thickness. The testing parameters here included a clamp speed of 50 mm/min and a load cell with a maximum capacity of 1000 kg.

3. Results and Discussion

3.1. Synthesis of UiO-66 MOFs

UiO-66 MOFs were successfully synthesized using a solvothermal method at 120°C for 24 hours. This synthesis

technique is acknowledged for producing high-quality MOF structures although it requires extended reaction times and elevated temperatures. The process involved the combination of zirconium chloride ($ZrCl_4$) and 1,4-benzenedicarboxylate (H_2BDC), which were dissolved in N,N-dimethylformamide (DMF) in an inert atmosphere within a nitrogen-filled glovebox.

Having completed synthesis, the UiO-66 product was washed with chloroform ($CHCl_3$) to remove any residual H_2BDC ligands and to replace the DMF solvent [8]. To eliminate any remaining DMF coordinated within the UiO-66 framework and activate the open metal sites (OMSs), a degassing process was carried out by heating the material to 250°C under vacuum. In this synthesis, DMF played a crucial role in protonating the H_2BDC ligand, allowing it to form complex bonds with the zirconium metal ions (Zr(IV)) [15].

The H_2BDC ligand contains carboxylate groups that become protonated by the oxygen in the carbonyl group of DMF, forming the carboxylate anions. These anions facilitate the bonding of H_2BDC to zirconium metal ions. Furthermore, DMF serves as a template for pore formation in the MOFs [9,1]. The choice of solvent and ligand is vital in determining the pore size of MOFs [14]; larger or more abundant ligands and solvent molecules tend to produce larger pores [16]. In this recent study, the synthesized UiO-66 MOFs were characterized using X-Ray Diffraction (XRD) and Fourier-Transform Infrared Spectroscopy (FTIR).

3.2. Synthesis of UiO-66/PEO/PVA polymer composite membrane

The UiO-66/PEO/PVA polymer composite membrane was synthesized using the solution casting method, known for its simplicity and effectiveness in combining multiple polymers. A key aspect of this method is the cautious selection of suitable solvents and polymers; hence, choosing an appropriate solvent for the polymers is deemed crucial.

In this study, the synthesis of the composite membrane involved the synthesized metal-organic frameworks (MOFs) known as UiO-66, along with the polymers polyethylene oxide (PEO) and polyvinyl alcohol (PVA), a solvent of distilled water, and lithium hexafluorophosphate ($LiPF_6$) salt. Distilled water was selected as the solvent due to the polar nature of PEO and PVA [15] that can make it effective for dissolving both polymers. The addition of $LiPF_6$ salt serves several purposes: providing high ionic conductivity [17,18], enhancing the thermal and chemical stability of the composite membrane [19], and reducing the internal resistance of the membrane [20].

During the experiment, the UiO-66/PEO/PVA composite membrane containing $LiPF_6$ salt was successfully synthesized by varying the amount of UiO-66 MOFs. Fig. 1 portrays the PEO/PVA and UiO-66/PEO/PVA composite membrane with $LiPF_6$ salt. However, despite successfully producing the UiO-66/PEO/PVA polymer composite membrane, agglomeration of the UiO-66 MOFs occurred during the synthesis in an open environment at room temperature. This led to non-ideal solvent evaporation, and resulted in an uneven distribution of the MOFs. To address this issue, a preventive measure was implemented to achieve a homogeneous UiO-66/PEO/PVA composite membrane that is by facilitating the evaporation process in a vacuum environment, which resulted in a uniformly distributed UiO-66/PEO/PVA composite membrane.

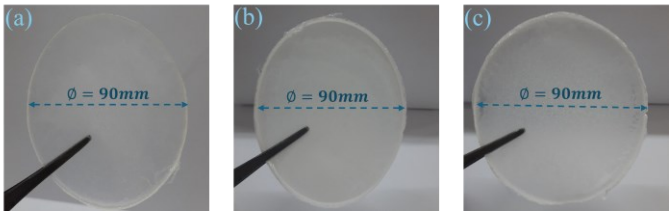

Fig. 1. Composite membranes of (a) PEO/PVA; (b) 2% UiO-66/PEO/PVA; (c) 8% UiO-66/POE/PVA

UiO-66 was evenly distributed throughout the composite membrane with little evidence of agglomeration. This indicated that the vacuum evaporation process effectively promoted the distribution of metal-organic frameworks (MOFs) within the PEO/PVA composite. The uniform distribution of UiO-66 was anticipated to improve the membrane's conductivity while maintaining its tensile strength.

3.3. Crystallinity analysis

The synthesized UiO-66 metal-organic frameworks (MOFs) and the UiO-66/PEO/PVA polymer composite membrane in this study were characterized by means of X-ray diffraction (XRD) aimed to validate the synthesis of the UiO-66 MOFs by analyzing their crystal structure, as well as to examine the crystal structure of the PEO/PVA polymer blend membrane. Fig. 2 displays the diffractogram of the synthesized UiO-66 MOFs. In this diffractogram, characteristic peaks were observed at 2θ values of 7.4°, 8.5°, 12.2°, and 25.9°. These peaks correspond to those reported in the literature [29], confirming that the UiO-66 MOFs have been successfully synthesized.

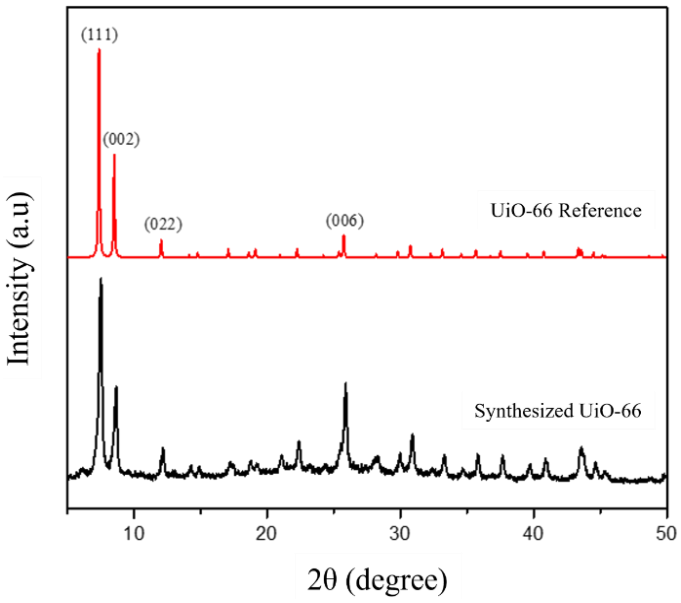

Fig. 2. Diffractogram of synthesized UiO-66 MOFs

The UiO-66/PEO/PVA polymer composite membrane was characterized using X-ray diffraction. Fig. 3 visualizes the

diffractogram of the synthesized membrane with the results showing that blending PEO with PVA led to a decrease in crystallinity, suggesting the formation of an amorphous phase [22].

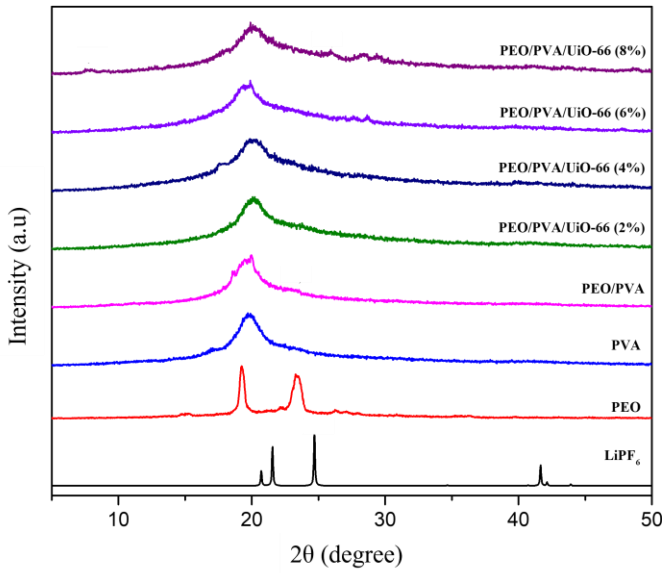

Fig. 3. Diffractogram of $LiPF_6$, PEO, PVA, and various additions of UiO-66 MOFs in the UiO-66/PEO/PVA polymer composite membrane

The characteristic peak of PEO in the PEO/PVA polymer blend, as observed at 2θ = 23.2°, showed very low intensity due to the 1:4 ratio of PEO to PVA. PVA is an amorphous polymer that acts as a plasticizer, further reducing the crystallinity of PEO [22,23]. In the diffractogram, the addition of 8% metal-organic frameworks (MOFs) revealed a characteristic peak of UiO-66 MOFs at 2θ = 7.6° though its intensity was also quite low. Furthermore, the peak of the lithium salt $LiPF_6$ in the polymer composite containing 8% MOFs appeared at 2θ = 25.9°, indicating a shift from the characteristic $LiPF_6$ peak at 2θ = 24.7°. This shift was likely due to the formation of complex bonds between the lithium salt and the open metal sites (OMSs) on the MOFs, resulting in the creation of ion channels [28,29,30].

3.4. Functional group analysis

FTIR analysis was made to gain information about the chemical structure by examining the IR absorption of functional groups. The IR spectrum of UiO-66 MOF was compared with that of the H_2BDC ligand to confirm the structure of UiO-66 MOFs. Fig. 4 illustrates the spectra for both UiO-66 MOFs and H_2BDC. The spectrum revealed an IR absorption band at 3394 cm^{-1}, indicating the presence of O–H groups [24,25]. Additionally, an absorption band at 1661 cm^{-1} was observed, which corresponded to C=O groups [28].

The peaks observed at 1402 cm^{-1} and 776 cm^{-1} indicated the presence of aromatic C–O and C–H groups, respectively [30]. As shown in Fig. 4, the IR absorption peaks of UiO-66 MOFs closely resembled those of H_2BDC; it suggested that the synthesized UiO-66 MOFs contained similar functional groups to those in H_2BDC. Also, there were noticeable shifts in the IR absorption peaks between the UiO-66 MOFs and H_2BDC. These shifts can be attributed to the coordination bonds formed between the zirconium metal (Zr) in the MOFs and the C=O functional groups [17]. For instance, the C=O absorption band in H_2BDC appeared at 1714 cm^{-1}, while in UiO-66 MOFs, it was observed at 1661 cm^{-1}. Another significant feature in the IR spectrum of UiO-66 MOFs was the absorption peak at 665 cm^{-1}, indicating the presence of Zr–O bonds [21].

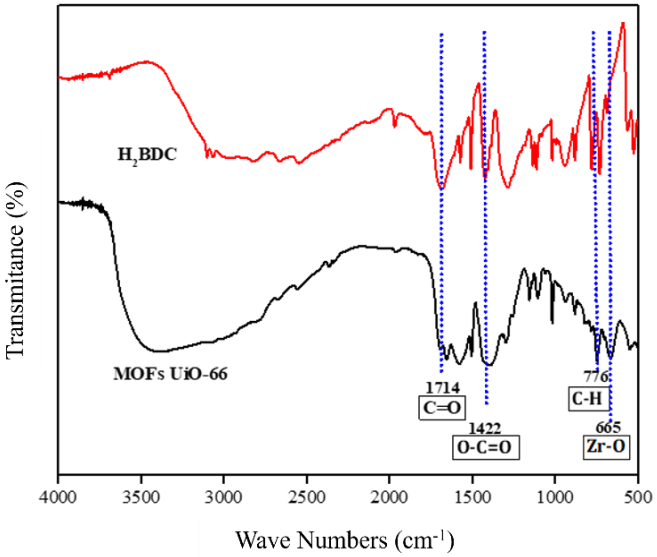

Fig. 4. IR Spectrum of UiO-66 MOFs and H_2BDC

FTIR characterization was also conducted to analyze the chemical structure of the polymer composite membrane. Fig. 5 displays the FTIR spectra of PEO, PVA, and the UiO-66/PEO/PVA polymer composite membrane. This spectrum provides detailed information about the absorption peaks corresponding to the functional groups present in the polymers, specifically the C–H, O–H, and C–O groups.

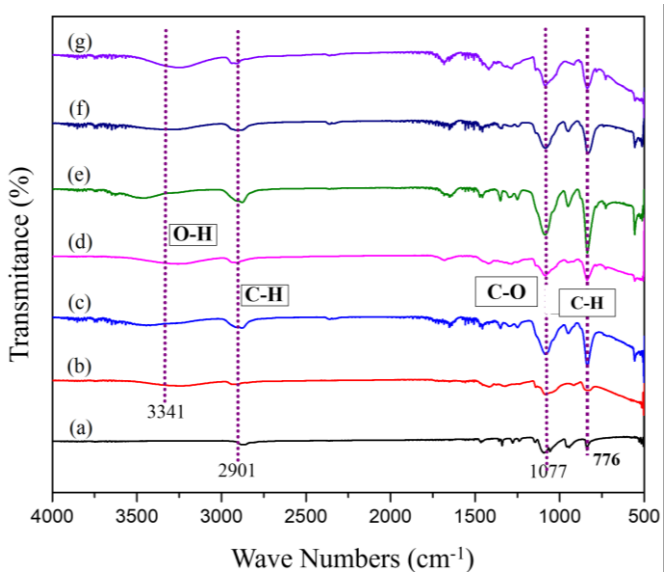

Fig. 5. IR Spectrum: (a) PEO; (b) PVA; (c) PEO/PVA; (d) PEO/PVA/UiO-66 (2%); (e) PEO/PVA/UiO-66 (4%); (f) PEO/PVA/UiO-66 (6%); and (g) PEO/PVA/UiO-66 (8%)

The differences in absorption peaks between PEO (Polyethylene Oxide) and PVA (Polyvinyl Alcohol) were

found obvious. PEO lacked an –OH absorption peak at 3341 cm^{-1}, while it featured a C–O peak at 1077 cm^{-1}. In the polymer blend of PEO and PVA, the appearance of distinct C–O and O–H absorption peaks indicated that PEO has been successfully combined with PVA. Variations in the intensity of these peaks suggested that the membrane transitioned toward an amorphous state, which aligned with the interpretations of its crystallinity [19, 20]. Conversely, the C–H peak at 2901 cm^{-1} reflected the presence of alkyl chains in the PEO/PVA polymer composite. These alkyl chains may contribute beneficial mechanical properties for battery applications [29]. Furthermore, the peak at 776 cm^{-1} became more pronounced with the increasing amount of UiO-66 added, denoting the presence of aromatic C–H groups within UiO-66. The presence of these C–H groups is able to foster the development of active sites, thereby enhancing ion migration [30].

3.5. Conductivity analysis

Electrochemical Impedance Spectroscopy (EIS) refers to a technique to examine the electrical properties of materials and electrode systems by measuring their impedance response to various frequencies of applied electrical signals. One common representation of EIS data is the Nyquist curve, featuring the resistive component (Z_{real}) on the *x*-axis and the reactive component ($-Z_{imag}$) on the *y*-axis. The shape of the resulting curve provides several valuable insights into the ion conduction mechanisms within the material. In membrane impedance analysis, the Nyquist curve is used to assess conductivity by identifying key parameters such as resistance and capacitance through the fitting of data to an equivalent circuit model. The commonly used equivalent circuits include elements such as bulk phase membrane resistance (R_s), charge transfer resistance (R_{ct}), Warburg conductance (W), and admittance conductance (Y_o).

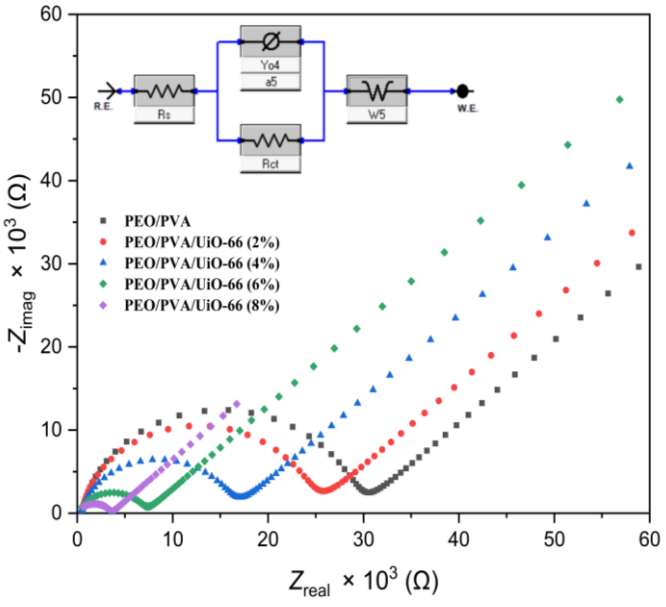

Fig. 6. Nyquist plot and equivalent circuit of UiO-66/PEO/PVA polymer membrane with $LiPF_6$ electrolyte and equivalent circuit

By analyzing the components of the equivalent circuit, it is possible to achieve a deeper understanding of the ion transport mechanisms and the contributions of each element to the overall impedance. Fig. 6 illustrates the Nyquist plot and the equivalent circuit used for the impedance measurements of PEO/PVA composites with varying UiO-66 contents.

As portrayed in Fig. 6, the PEO/PVA composites exhibited a larger semicircle shape compared to PEO/PVA composites including UiO-66. This indicated that the capacitance (which correlated with Y_o) of PEO/PVA without UiO-66 was higher than that of PEO/PVA in that the content of UiO-66 increased. In any battery applications, a composite membrane is considered more effective if it has lower capacitance or reduced charge storage capacity [23]. Therefore, PEO/PVA/UiO-66 commonly is regarded as superior to PEO/PVA vis-à-vis capacitance. However, both PEO/PVA and PEO/PVA/UiO-66 demonstrated ion diffusion activity, as evidenced by the semicircle tail in the Nyquist plot, represented by the Warburg element (W) in the equivalent circuit [16]. Additionally, key parameters such as R_{ct}, R_s, and σ are important. The parameter σ is directly proportional to the membrane thickness and inversely proportional to R_{ct} as well as the effective contact area of the membrane.

Table 1 depicts the values of R_{ct}, R_s, and σ obtained from the EIS measurements of PEO/PVA composite membranes with the varying concentrations of UiO-66.

Table 1. Values of R_s, R_{ct}, and σ from EIS testing of polymer composite membranes with various UiO-66 MOF contents

Composites	R_s (Ω)	R_{ct} (Ω)	(σ) (S cm^{-1})
PEO/PVA	501	28750	1.30×10^{-3}
PEO/PVA/UiO-66 (2%)	454	24000	1.56×10^{-3}
PEO/PVA/UiO-66 (4%)	300	15840	2.37×10^{-3}
PEO/PVA/UiO-66 (6%)	126	6996	5.36×10^{-3}
PEO/PVA/UiO-66 (8%)	4.3×10^{-8}	3576	10.49×10^{-3}

Table 1 shows that incorporating UiO-66 into the PEO/PVA membrane led to a reduction in the R_s value. This reduction indicated that the addition of UiO-66 enhanced the charge transport rate within the membrane. Separator membranes with a low R_s value mostly contribute to a longer battery lifespan by decreasing heat generation during charging and discharging processes [8,14]. In addition to lower the R_s value, the addition of UiO-66 to the PEO/PVA membrane also reduces the R_{ct} value. This implies that electron transfer between anode and cathode becomes more efficient, thereby improving the overall performance and reliability of the battery [19]. A decrease in R_{ct} directly impacts the ionic conductivity (σ), resulting in an increase in σ when UiO-66 is added. This increase indicates that UiO-66 facilitates the movement of charge through the membrane, allowing for efficient transfer between electrodes during both charging and discharging [30].

Overall, the incorporation of UiO-66 into the PEO/PVA composite membrane provides significant benefits for battery applications. This can be attributed to the strong interaction between UiO-66 and the PEO/PVA polymer matrix, as proven by the IR peak at 776 cm^{-1} corresponding to C–H bonds [4,5]. This interaction contributes to the formation of more efficient

ionic pathways and enhances ion mobility within the membrane. Furthermore, the addition of UiO-66 improves the structural stability of the membrane, facilitating to maintain stable ionic pathways throughout the charging and discharging cycles [9]. The Zr-O bonds in UiO-66 can also serve as the active sites for ion transport, increasing the number of conductive sites within the membrane and enhancing ion transfer capabilities. The combined effects of PEO/PVA, $LiPF_6$, and UiO-66 result in increased ionic conductivity and decreased overall resistance, ultimately leading to improved battery performance.

3.6. Mechanical testing of UiO-66/PEO/PVA polymer composite membrane

Understanding the mechanical properties of polymer composite membranes is essential to produce separators used in lithium-ion batteries. The polymer membrane should not be rigid, brittle, or excessively thick [38]; it must be both elastic and strong during the production process and battery assembly [35]. The mechanical properties of the UiO-66/PEO/PVA polymer composite membrane were evaluated using a TENSOLAB-5000 at room temperature. Fig. 7 displays the results of the tensile tests performed on the UiO-66/PEO/PVA polymer composite membrane, while Table 2 summarizes the tensile strength and strain values for this membrane.

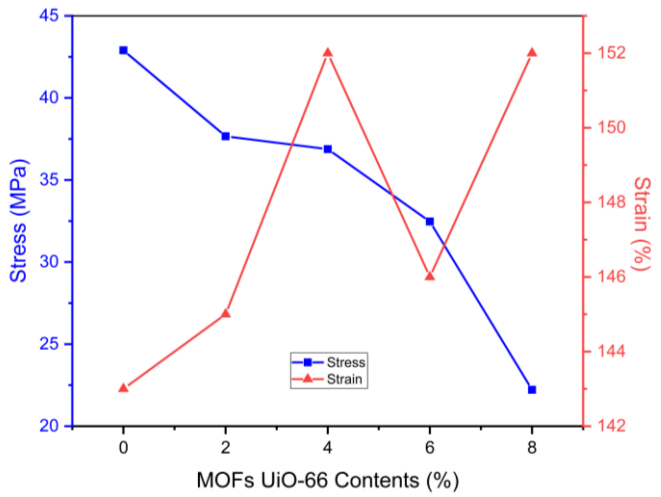

Fig. 7. Tensile strength and strain curve of the MOFs UiO-66/PEO/PVA polymer composite membrane with different MOFs UiO-66 contents

Table 2. Tensile strength and strain of the MOFs UiO-66/PEO/PVA polymer composite membrane with various MOFs UiO-66 concentrations

Composites	Thickness (mm)	Tensile Strength (MPa)	Strain (%)
PEO/PVA	9×10^{-2}	42.9	143
PEO/PVA/UiO-66 (2%)	10×10^{-2}	37.7	145
PEO/PVA/UiO-66 (4%)	11×10^{-2}	36.9	152
PEO/PVA/UiO-66 (6%)	11×10^{-2}	32.5	146
PEO/PVA/UiO-66 (8%)	10×10^{-2}	22.2	152

When poly(ethylene oxide) (PEO) was blended with poly(vinyl alcohol) (PVA), the resultant polymer membrane demonstrated a tensile strength of 42.9 MPa, even without the inclusion of UiO-66. This enhanced strength was attributed to the hydrogen bonds formed between the hydroxyl groups of PVA and the ether groups of PEO that increased the membrane's rigidity [14]. However, adding UiO-66 significantly decreased the tensile strength of the polymer electrolyte membrane to 22.2 MPa when 8% UiO-66 was incorporated. This reduction is consistent with crystallinity analyses showing an amorphous structure owned by the composite membrane. The presence of the rigid UiO-66 structure is able to disrupt the uniformity of the PEO/PVA matrix, ultimately weakening the tensile strength [15]. Interestingly, when 6% UiO-66 was added, the composite membrane exhibited a tensile strength of 32.5 MPa. This indicated that the level of UiO-66 inclusion still resulted in a membrane suitable for battery applications, requiring a minimum tensile strength of 30 MPa [38].

Additionally, incorporating UiO-66 enhances the elasticity of the polymer composite membrane. The strain increased from 143% (with 0% UiO-66) to 152% (with 8% UiO-66), implying that the addition of UiO-66 can improve the membrane's elasticity, probably in view of the UiO-66 particles creating voids within the polymer matrix that permit greater deformation [37]. However, the decrease in strain observed with the addition of 6% UiO-66 can be attributed to sensitivity to humidity determined by the presence of the lithium salt $LiPF_6$. Although an 8% concentration of UiO-66 offered good conductivity, it resulted in a tensile strength below 30 MPa. This showed that 8% UiO-66 was not optimal for maintaining tensile strength, while a 6% concentration proved to be ideal. In conclusion, while the addition of UiO-66 commonly reduces tensile strength, it can also result in fluctuations in strain. Table 3 presents a comparison of the conductivity and mechanical properties of various PEO/PVA composite membranes designed for battery applications.

Table 3. The conductivity and tensile strength values of composite membranes based on PEO and PVA for application in batteries.

Composites	(σ) (S cm^{-1})	Tensile Strength (MPa)	REF
PEO/PVA/$LiClO_4$	3.5×10^{-3}	(none)	[19]
Celgard/LNS/Li-S	$0{,}56 \times 10^{-3}$	(none)	[29]
PEO/PVA/GO/ $LiClO_4$	1.65×10^{-3}	4.4	[30]
PEO/PVA/FGO/ $LiClO_4$	5.20×10^{-5}	13.6	[31]
PEO/PVA/PESf/ $LiFPO_4$	0.83×10^{-3}	(none)	[32]
PVA/ $LiClO_4$/CNC	1.31×10^{-4}	36.6	[33]
PEO/T/PVDF/LiTFSI	2.46×10^{-9}	(none)	[22]
PEO/Li_6PS_5Cl	1.03×10^{-3}	50	[23]
PVA/CS/ $LiClO_4$	0.846×10^{-3}	(none)	[34]
Celgard/ $LiPF_6$	2.80×10^{-3}	(none)	[40]
PEO/PVA/UiO-66/ $LiPF_6$	5.60×10^{-3}	32.5	This Work

The optimal content of UiO-66 metal-organic frameworks (MOFs) for this polymer composite membrane was determined to be 6% w/w. This positioned it as a promising alternative to Celgard for lithium-ion battery separators. The

mini-research conducted, as depicted in Table 3, showed that the conductivity and tensile strength of the PEO/PVA/UiO-66 composite were competitive with those of other PEO/PVA and Celgard composites used in battery applications. This improved performance was primarily attributed to the addition of UiO-66 MOFs at the optimal concentration, as demonstrated by our research. Additionally, we believe that the type of lithium salt utilized may have contributed to enhancing conductivity since its anion differs from those found in the lithium salts used in other studies [41].

4. Conclusion

Characterization techniques, including X-ray diffraction and FTIR, confirmed the successful synthesis of the metal-organic framework (MOF) UiO-66 through solvothermal methods. The X-ray diffraction analysis of the UiO-66 polymer composite membrane indicated the formation of an amorphous phase. Meanwhile, FTIR analysis confirmed the effective blending of polyethylene oxide (PEO) and polyvinyl alcohol (PVA) through solution casting. Electrochemical impedance spectroscopy (EIS) revealed that increasing the content of UiO-66 reduced resistance and enhanced ionic conductivity. Meanwhile, mechanical testing showed that the addition of UiO-66 increased the strain at break but decreased the tensile strength. The optimal UiO-66 content was observed at 6% w/w that achieved an ionic conductivity of 5.36×10^{-3} S cm^{-1} and a tensile strength of 32.5 MPa.

Acknowledgements

DR expresses his sincere gratitude to the Indonesia Endowment Fund for Education, under the Ministry of Finance (LPDP), and the Higher Education Funding Agency (BPPT-BPI) of the Republic of Indonesia for their invaluable moral and material support, making the completion of this paper possible.

References

1. J. Yuan, X. Shi, Q. Qiu, P. Yao, Y. Xia, Y. Zhao, and Y. Li, *Ion selective bifunctional metal-organic framework-based membrane for lithium metal-based nonaqueous redox flow battery,* ACS Appl. Energy Mater. 6 (2023) 416–423.
2. X. Feng, N. Deng, W. Yu, Z. Peng, D. Su, W. Kang, and B. Cheng, *Review: application of bionic-structured materials in solid-state electrolytes for high-performance lithium metal batteries,* ACS Nano 18 (2024) 15387–15415.
3. M. A. Mushtaq, M. Ahmad, A. Shaheen, A. Mehmood, G. Yasin, M. Arif, Z. Ali, P. Li, S. N., Hussain, M. Tabish, A. Kumar, S. Ajmal, W. Raza, M. Akhtar, A. Saad, and D. Yan, *Advancing the development of hollow micro/nanostructured materials for electrocatalytic water splitting: current state, challenges, and perspectives*, ACS Materials Lett. 6 (2024) 3090–3111.
4. Y. Zhang, J. Guo, M. Yu, X. Li, S. Liu, H. Song, W. Wu, C. Zheng, and X. Gao, *Selective lithium leaching from spent lithium-ion batteries via a combination of reduction roasting and mechanochemical activation*, ACS Sustainable Chem. Eng. 12 (2024) 6629–6639.
5. R. Abdullah, D. Astira, U. Zulfiani, A. R. Widyanto, Z. Rahmawati, T. Gunawan, Y. Kusumawati, M. H. D. Othman, and H. Fansuri, *Ultrafiltration membranes for dye wastewater treatment: Utilizing cellulose acetate and microcrystalline cellulose fillers from Ceiba Pentandra,* Communications in Science and Technology 9(1) (2024) 7–15.
6. M. Yuan, S. Zhang, L. Lin, Z. Sun, H. Yang, H. Li, G. Sun, C. Nan, and S. Ma, *Manganese carbodiimide nanoparticles modified with N-doping carbon: a bifunctional cathode electrocatalyst for aprotic Li-O_2 Battery,* ACS Sustainable Chem. Eng. 7 (2019) 17464–17473.
7. A. Kahfi, N. Kusumawati, P. Setiarso, S. Muslim, S. A. Cahyani, and N. Zakiyah, *Study in the impact of quaternized graphene oxide (QGO) composition as modifier on the chemical, physical, mechanical, and performance properties of polyvinylidene fluoride (PVDF)-based nanocomposite membran*e, Communications in Science and Technology 9(1) (2024) 30–37.
8. S. Bandyopadhyay, N. Gupta, A. Joshi, A. Gupta, R. K. Srivastava, B. K. Kuila, and B. Nandan, *Solid polymer electrolyte based on an ionically conducting unique organic polymer framework for all-solid-state lithium batteries*, ACS Appl. Energy Mater. 6 (2023) 4390–4403.
9. B. Zhong, C. Liu, D. Xiong, J. Cai, J. Li, D. Li, Z. Cao, B. Song, W. Deng, H. Peng, H. Hou, G. Zou, and X. Ji, *Biomass-derived hard carbon for sodium-ion batteries: basic research and industrial application*, ACS Nano 18 (2024) 16468–16488.
10. H. Bao, D. Chen, B. Liao, Y. Yi, R. Liu, and Y. Sun, *Enhanced ionic conduction in metal-organic-framework-based quasi-solid-state electrolytes: mechanistic insights,* Energy and Fuels 38 (2024) 11275–11283.
11. B. M. Wiers, M. L. Foo, N. P. Balsara, and J. R. Long, *A solid lithium electrolyte via addition of lithium isopropoxide to a metal-organic framework with open metal sites,* J. Am. Chem. Soc. 133 (2011) 14522–14525.
12. T. Zhou, W. Wang, H. Luo, Y. Wu, R. Xia, Y. Zhang, Z. Li, G. Jia, T. Zhang, H. Peng, and Z. Guo, *Asymmetrical Ru-O-Mn bridge active sites fully decouple bifunctional oxygen electrocatalysis for rechargeable zinc-air batteries,* ACS Catal. 14 (2024) 9313–9322.
13. Y. Xia, N. Xu, L. Du, Y. Cheng, S. Lei, S. Li, X. Liao, W. Shi, L. Xu, and L. Mai, *Rational design of ion transport paths at the interface of metal-organic framework modified solid electrolyte,* ACS Appl. Mater. Interfaces 12 (2020) 22930–22938.
14. J. Liu, Q. Sun, Q. Ye, J. Chen, Y. Wu, Y. Ge, L. Zhang, Z. Yang, and J. Qian, *MOF-derived cobalt nanoparticles with dispersed iron phthalocyanines as bifunctional oxygen electrocatalysts*, ACS Sustainable Chem. Eng. 12 (2024) 4779–4788.
15. R. Lin, Y. Jin, X. Zhang, Y. Li, Y. Zhang, and Y. Xiong, *Hierarchical bulk-interface design of MOFs framework for polymer electrolyte towards ultra-stable quasi-solid-state Li metal batteries,* Chem. Eng. J. 479 (2024) 147558-147570.
16. K. Zhang, X. Qian, L. Jin, Q. Hao, S. Zhao, B. Li, S. Pang, and X. Shen, *Application of Sn-MOF-derived SnO_2 and SnO_2/CNTs composites in separator modification for lithium-sulfur batteries*, J. Electroanal. Chem. 947 (2023) 117782-117790.
17. H. Zhu, S. Li, L. Peng, W. Zhong, Q. Wu, S. Cheng, and J. Xie, *Review of MOF-guided ion transport for lithium metal battery electrolytes,* Nano Energy. 125 (2024) 109571-109595.
18. S. H. Kang, H. Y. Jeong, T. H. Kim, J. Y. Lee, S. K. Hong, J. Choi, S. So, S. J. Yoon, and D. M. Yu, *Aluminum diethylphosphinate-incorporated flame-retardant polyacrylonitrile separators for safety of lithium-ion batteries,* Polymers. 14 (2022) 1649-1661.
19. B. Jinisha, A. F. Femy, M. S. Ashima, and S. Jayalekshmi, *Polyethylene oxide (PEO) / polyvinyl alcohol (PVA) complexed with lithium perchlorate ($LiClO_4$) as a prospective material for making solid polymer electrolyte films*, Mater. Today: Proceedings. 5 (2018) 21189–21194.
20. A. R. Polu, P. K. Singh, P. S. Kumar, G. M. Joshi, T. Ramesh, I. M. Noor, A. Y. Madkhli, and S. Kakroo, *Development of solid polymer electrolytes based on poly (ethylene oxide) complexed with 2-trifluoromethyl-4, 5-dicyanoimidazole lithium salt and 1-ethyl-3-methylimidazolium bis(trifluoromethylsulfonyl)imide ionic liquid for Li-ion batteries*, High Performance Polymer. 35 (2023) 4–9.
21. M. Dmitrenko, A. Chapeleva, V. Liamin, A. Mazur, K. Samenov, N. Solovyev, and A. Penkova., *Novel mixed matrix membranes based on polyphenylene oxide modified with graphene oxide for enhanced pervaporation dehydration of ethylene glycol*, Polymers. 14 (2022) 691-714.

22. L. Gao, J. Li, J. Ju, L. Wang, J. Yan, B. Cheng, W. Kang, N. Deng, and Y. Li., *Designing of root-soil-like polyethylene oxide-based composite electrolyte for dendrite-free and long-cycling all-solid-state lithium metal batteries*, Chem. Eng. J. 389 (2020) 124478-124490.
23. J. Zhang, C. Zheng, J. Lou, Y. Xia, C. Liang, H. Huang, Y. Gan, X. Tao, and W. Zhang., *Poly(ethylene oxide) reinforced Li_6PS_5Cl composite solid electrolyte for all-solid-state lithium battery: Enhanced electrochemical performance, mechanical property and interfacial stability,* J. Power Source. 412 (2019) 78–85.
24. C. Bai, Z. Wu, W. Xiang, G. Wang, Y. Liu, Y. Zhong, B. Chen, R. Liu, F. He, and X. Guo., *Poly(ethylene oxide)/poly(vinylidene fluoride)/$Li_{6.4}La_3Zr_{1.4}Ta_{0.6}O_{12}$ composite electrolyte with a stable interface for high performance solid state lithium metal batteries,* J. Power Source. 472 (2020) 228461-228469.
25. F.H. Abd El-Kader, N.A. Hakeem, I.S. Elashmawi, and A.M. Ismail. *Enhancement of structural and thermal properties of PEO/PVA blend embedded with TiO_2 nanoparticles,* Indian J. Phys. 87 (2013) 983–990.
26. H.M. Ragab. *The influence of graphene oxide on the optical, thermal, electrical, and dielectric properties of PVA/PEO composite,* J. Mater. Sci: Mater Electron. 33 (2022) 19793–19804.
27. M. Brza, S. B. Aziz, S. R. Saeed, M. H. Hamsan, S. R. Majid, M. F. Z. Kadir, and R. M. Abdullah., *Energy storage behavior of lithium-ion conducting poly(Vinyl alcohol) (PVA): Chitosan(CS)-based polymer blend electrolyte membranes: Preparation, equivalent circuit modeling, ion transport parameters, and dielectric properties,* Membranes 10 (2020) 381-401.
28. Q. Yang, J. Guo, S. Zhang, F. Guan, Y. Yu, S. Feng, X. Song, D. Bao, and X. Zhang, *Development of cell adhesive and inherently antibacterial polyvinyl alcohol/polyethylene oxide nanofiber scaffolds via incorporating chitosan for tissue engineering,* Int. J. Biol. Macromol. 236 (2023) 124004-124013.
29. Y. Yang, and J. Zhang., *Highly stable lithium–sulfur batteries based on laponite nanosheet-coated Celgard separators*, Adv. Energy Mater. 180778 (2018) 1801778.
30. S. Hasanpoor, I. Ghasemi, and S. Gomari., *Ionic conductivity and mechanical properties of semi-interpenetrating networks based on poly(ethylene oxide)/polyvinyl alcohol/graphene oxide: a response surface methodology study,* Iran. Polym. J. (English Edition). 33 (2024) 567–579.
31. B. Eslami, I. Ghasemi, and M. Esfandeh., *Using pegylated graphene oxide to achieve high performance solid polymer electrolyte based on poly(ethylene oxide)/polyvinyl alcohol blend (PEO/PVA)*, Polymers 15 (2023) 3063-3078.
32. L. Xu, K. Wei, Y. Cao, S. Ma, J. Li, Y. Zhao, Y. Cui, and Y.Cui., *The synergistic effect of the PEO-PVA-PESf composite polymer electrolyte for all-solid-state lithium-ion batteries,* RSC Adv. 10 (2020) 5462–5467.
33. E. Purwanti, D. Wahyuningrum, A. Rochliadi, and I. M. Arcana, *Polymer electrolyte membrane based on PVA/$LiClO_4$ nanocomposite reinforced cellulose nanocrystalline from corncob for lithium-ion battery*, J. Polym. Sci. 62 (2024) 1424–1436.
34. R. Rusli, I. Abrahams, A. Patah, B. Prijamboedi, and Ismunandar, *Ionic conductivity of $Bi_2Ni_xV_{1-x}O_{5.5-3x/2}$ ($0.1 \leq x \leq 0.2$) oxides prepared by a low temperature sol-gel route,* AIP Conf. Proc. 1589 (2014) 178–181.
35. M. Kandiah, M. H. Nilsen, S. Usseglio, S. Jakobsen, U. Olsbye, M. Tilset, C. Larabi, E. Alessandra, F. Bonino, and K. P. Lillerud., *Synthesis and stability of tagged UiO-66 Zr-MOFs,* Chem. Mater. 22 (2010) 6632–6640.
36. S. Xu, Q. Gao, C. Zhou, J. Li, L. Shen, and H. Lin, *Improved thermal stability and heat-aging resistance of silicone rubber via incorporation of UiO-66-NH_2*, Mater. Chem. Phys. 274 (2021) 125182-125189.
37. G.C. Shearer, S. Chavan, S. Bordiga, S. Svelle, U. Olsbye, and K.P. Lillerud, *Defect Engineering: Tuning the porosity and composition of the metal-organic framework UiO-66 via modulated synthesis*, Chem. Mater. 28 (2016) 3749–3761.
38. D. Ma, S.B. Peh, G. Han, and S.B. Chen. *Thin-film nanocomposite (TFN) membranes incorporated with super-hydrophilic metal-organic framework (MOF) UiO-66: Toward enhancement of water flux and salt rejection*, ACS Appl. Mater. Interfaces 9 (2017) 7523–7534.
39. C. Cao, F. Liu, F. Li, O.R. Uzochukwu, and Chen L. *A novel strategy for retarding membrane wetting under electrical field: Embedding silver nanowires into UiO-66-NH_2/graphene oxide composite thin membrane*, Desalination 574 (2024) 117263-117276.
40. S.H. Wang, S.S. Hou, P.L. Kuo, and H. Teng, *Poly(ethylene oxide)-co-poly(propylene oxide)-based gel electrolyte with high ionic conductivity and mechanical integrity for lithium-ion batteries,* ACS Appl. Mater. Interfaces 11 (2013) 8477–8485.
41. A. Patah, Y. Rachmawati, R. Utari, and A. Rochliadi. *Penentuan resistivitas tak-terkompensasi cairan ion berbasis imidazol dengan metode EIS: pengaruh panjang alkil dan perbedaan anion*, J. Ris. Kim. 11 (2020) 106–112.